Published in IET Microwaves, Antennas & Propagation
Received on 7th November 2010
Revised on 30th May 2011
doi: 10.1049/iet-map.2010.0545

ISSN 1751-8725

Compact multi-band printed dipole antenna loaded with single-cell metamaterial

M. Rafaei Booket[1] *A. Jafargholi*[2] *M. Kamyab*[2] *H. Eskandari*[3] *M. Veysi*[2] *S.M. Mousavi*[2]

[1]*School of Electrical and Computer Engineering, Tarbiat Modares University*
[2]*Electrical Engineering Department, K.N. Toosi University of Technology*
[3]*Urmia University*
E-mail: jafargholi@ee.kntu.ac.ir

Abstract: A compact multi-band printed dipole antenna loaded with reactive elements is proposed. The reactive loading of the dipole is inspired by the Epsilon–negative (ENG) and double negative metamaterial inclusions, which enable the loaded dipole to operate in multi-band. The reactive loads are realised by two rake-shaped split ring resonators facing each other. Investigations reveal that the loaded dipole radiates at two or three separated bands depending on symmetrical or asymmetrical loading and load locations. The new resonance frequencies are lower than the natural resonance frequency of the conventional half-wavelength dipole. In this range of frequencies, the radiation efficiency of the composite antenna is high. In order to validate the simulation results, a prototype of the proposed printed dipole is fabricated and tested. The agreement between the simulated and measured results is quite good.

1 Introduction

The increasing demands on compact multifunctional devices have necessitated the development of multi-frequency printed dipoles, which can be integrated into familiar devices such as laptop computers and mobile phones. The typical difficulties encountered in designing compact antennas include narrow bandwidth and low radiation efficiency. In order to achieve a good efficiency, considerable effort must be expended on the matching network. Other researchers have found that the bandwidth of the dipole antenna can be enhanced by loading the antenna with parallel lumped element circuits [1]. Over the last decade, increasing demands for low profile multifunctional antennas have resulted in considerable interest by the electromagnetic research community in metamaterials (MTMs). Owing to unique electromagnetic properties, MTMs have been widely considered in monopole and dipole antennas to improve their performance [2–5]. The applications of composite right/left handed (CRLH) structures to load the printed dipole have been investigated both numerically [6–8] and analytically [9]. However, main drawbacks of this method are low gain and low efficiency. The use of transmission-line-based MTMs to realise a tri-band monopole antenna has been recently investigated in [10]. However, the cross-polarisation levels of the proposed antenna in [10] are very high. It is also known that the antenna properties can be improved by covering the metal radiating parts or filling the antenna volume. For instance, the bandwidth of the microstrip patch antenna can be significantly improved by replacing the dielectric substrate with the magneto-dielectric one [11]. Recently, Ziolkowski and Kipple have considered the use of double negative (DNG) cover to match an electrically small electric dipole antenna to free space [3]. The effect of complex material coverings on the bandwidth of the antennas has been also investigated in [12].

In this paper, first, the effect of material inclusions embedded in a simple dipole antenna has been investigated. The numerical investigations result in some general conclusions regarding the effect of material inclusions on the dipole antenna performance. It is demonstrated that in contrast to the double-positive (DPS) and μ-negative (MNG) MTMs, ϵ-negative (ENG) and DNG-MTM inclusions can provide multi-band performance. To practically realise this method, a compact multi-band printed dipole antenna is designed using reactive loading, which is inspired by ENG-MTM inclusions. To this aim, a novel printed MTM element is proposed and successfully tested. The proposed MTM cell shows ENG behaviour at around the antenna-operating frequency. The dimensions of the proposed MTM cell is optimised to meet the specifications of the mobile bands (890.2–914.8 and 1710–1784 MHz) while maintaining its compact size. The antenna radiation efficiency at the first resonance frequency is significantly higher than those reported for other miniaturised printed dipoles in the literature [6–9]. It is worthwhile to point out here that the subject of single-cell MTM loading is not new and has been studied by other authors [10].

2 Dipole antenna loaded with MTM inclusions

The resonance frequencies of an original monopole/dipole are harmonics of the main resonant frequency ω_1. However, ominidirectional radiation pattern distortion and low directivity are two major disadvantages associated with

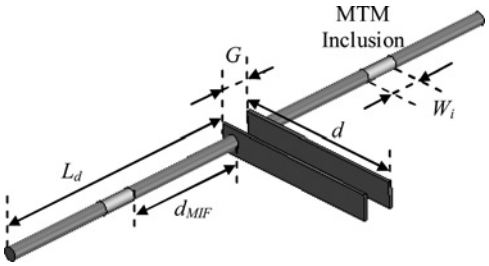

Fig. 1 *Ideal model of MTM-loaded dipole: $L_d = 120$ mm, $W_i = 2.5$ mm, $G = 5$ mm and $d = 27$ mm*

monopole/dipole antenna resonating at higher-order harmonics ($\omega_m > \omega_1$) [5, 13]. In this section, a simple and intuitive rule for determining the beneficial filling material type for dipole antennas has been introduced. A dipole antenna loaded with cylindrical dispersive MTM inclusions is shown in Fig. 1. It is assumed that the MTM inclusions are embedded in the both arms of the dipole. Here, the Drude model [14] is used to simulate the MTM inclusions, since it can yield a negative real part of the permittivity/permeablity over a wide frequency range. Depending on the MTM type either μ or ϵ (or both) obey the Drude model (with plasma frequency $\omega_p = 1.8 \times 10^{10}$ rad/s and collision frequency $f_c = 0.2$ GHz) and are equal to one otherwise. The distance from the location of the MTM inclusions to the feed point is denoted as d_{MIF}. The behaviours of the loaded dipole as a function of the MTM type and the distance of the MTM inclusions from the antenna feed point, d_{MIF}, have been studied. Fig. 2 shows the antenna return loss for the dipoles loaded with DPS-, MNG-, DNG- and ENG-inclusions, with d_{MIF} as a parameter. As the ENG- or DNG-inclusions are added, the antenna resonant behaviour changes. It can be concluded from Fig. 2 that for the dipole antenna loaded with DNG- or ENG-inclusions, an additional resonance frequency is introduced at the frequencies lower than the antenna resonant frequency where the antenna radiates an omnidirectional radiation pattern. In contrast, for the dipoles loaded with DPS- or MNG-inclusions, changing DPS/MNG locations on the antenna arms causes no resonance at frequencies lower than the main resonant frequency, as shown in Figs. 2*a* and *b*. As the distance between the ENG-/DNG-inclusions and the feed point is increased, the main resonant frequency decreases, whereas the low resonant frequency is almost unchanged. This feature provides the ability to choose the second resonance frequency arbitrarily based on provision dictated by application. Thus, the frequency ratio between these two frequencies can be readily controlled by adjusting the inclusion locations. In addition, for the case of the dipoles loaded with DNG-/ENG-blocks and $50 \text{ mm} < d_{MIF} < 75$ mm, more than one resonance is introduced at around the antenna main resonant frequency where the antenna radiates omnidirectional radiation patterns, as shown in Figs. 2*b* and *c*.

To make the concept more clear, three DNG-loaded dipoles are designed and simulated. The return loss results for the dipole antennas loaded with different DNG blocks and different d_{MIF} are shown in Fig. 3. For comparison

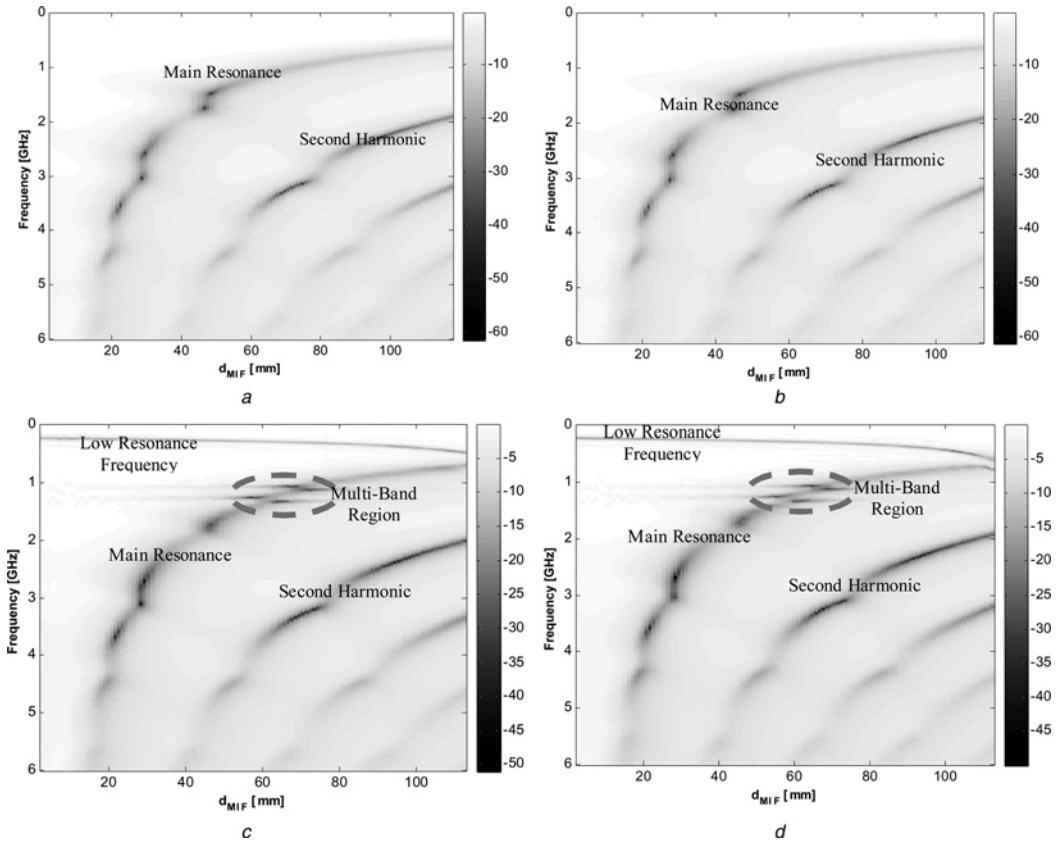

Fig. 2 *CST simulation results for $|S_{11}|$ (dB)*

a DPS-inclusions
b MNG-inclusions
c DNG-inclusions
d ENG-inclusions

doi: 10.1049/iet-map.2010.0545

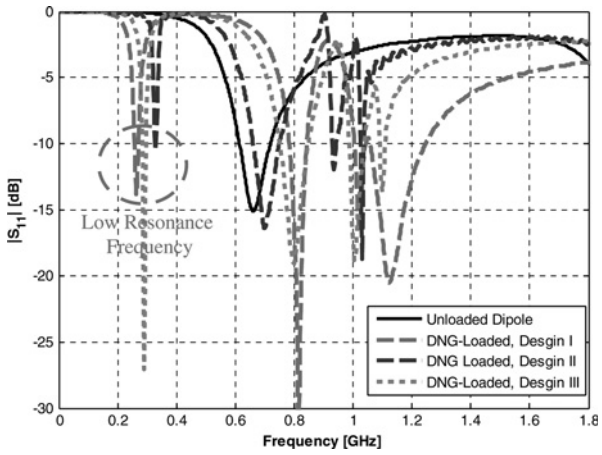

Fig. 3 *Return loss results for dipole antennas loaded with different DNG blocks*

As a reference, an unloaded dipole antenna is also simulated
Design I: $d_{MIF} = 72$ mm and Drude model with $\omega_p = 1.8 \times 10^{10}$ rad/s and $f_c = 0.2$ GHz, design II: $d_{MIF} = 100$ mm, $\omega_p = 1.8 \times 10^{10}$ rad/s and $f_c = 0.01$ GHz and design III: $d_{MIF} = 85$ mm, $\omega_p = 1.8 \times 10^{10}$ rad/s and $f_c = 0.1$ GHz

purposes, the return loss of an unloaded dipole antenna is also presented in Fig. 3. As can be seen, all the antennas have multi-resonance behaviour. The first frequency bands of the proposed loaded dipoles are narrow. This narrow frequency bands are the direct consequence of the resonant nature of the MTM inclusions. The gain, efficiency and bandwidth of the three loaded dipoles are compared in Table 1. For the first design, the antenna bandwidth at first resonance is quite good but its gain is low. In contrast, for the second design, the antenna has a high gain at the first resonance frequency but at the expense of a narrower bandwidth. As a result, the type of the DNG-inclusion is a result of a trade-off between the antenna radiation efficiency (gain) and bandwidth, such as design III.

3 Proposed printed MTM cell

In the previous section, it was revealed that the use of the ENG- and DNG-inclusions has led to a multi-resonance behaviour. In this section, a new printed MTM cell is introduced to realise the ENG-inclusions. Fig. 4 shows a schematic of the proposed MTM cell along with its design parameters. The proposed MTM cell is printed on an FR4 substrate with a thickness of 0.8 mm and a dielectric constant of 4.4. An important feature of the proposed MTM is that it offers more degrees of freedom than conventional MTM cells [14].

In order to retrieve the constitutive parameters of the proposed MTM, a unit cell positioned between two perfect electric conductors (PEC) in x-direction and two perfect magnetic conductors (PMC) in z-direction is simulated, and used to model an infinite periodic structure [15]. The

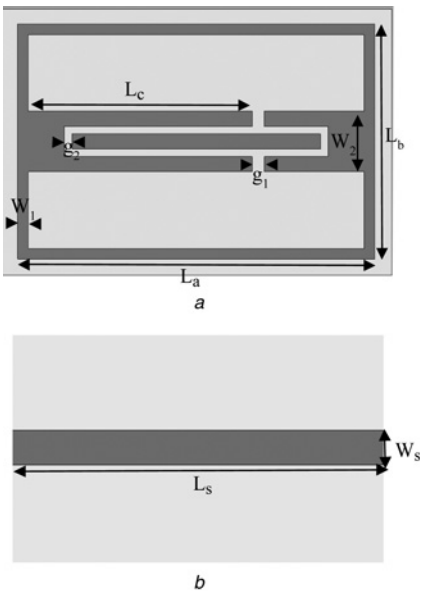

Fig. 4 *Schematic representation of the proposed MTM unit cell and its design parameters*

a Front view
b Back view: $L_a = 23.54$ mm, $L_b = 15.55$ mm, $L_c = 14.78$ mm, $w_1 = 0.7$ mm, $g_1 = 0.8$ mm, $w_2 = 4$ mm, $g_2 = 0.5$ mm, $w_s = 2.5$ mm and $L_s = 26.75$ mm

resultant scattering parameters obtained from CST microwave studio are exerted to the Chen's algorithm [15]. The normalised impedance (z) and refractive index (n) of the under-study medium can be calculated as following

$$z = \pm\sqrt{\frac{(1+s_{11})^2 - s_{21}^2}{(1-s_{11})^2 - s_{21}^2}}, \quad \text{real}(z) \geq 0 \tag{1}$$

$$n = \frac{1}{k_0 d}\{[\ln(e^{ink_0 d})]' + 2m\pi] - i[\ln(e^{ink_0 d})]'\} \tag{2}$$

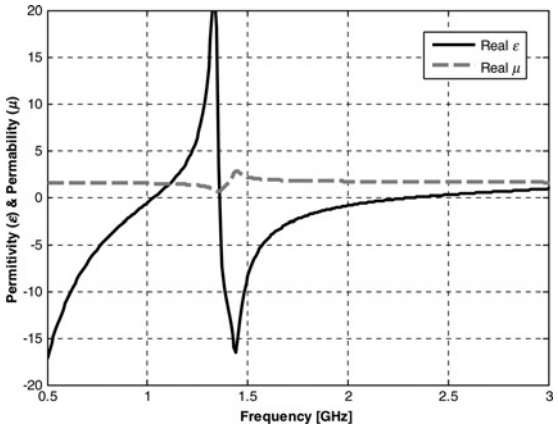

Fig. 5 *Retrieved effective parameters of the proposed MTM cell*

Table 1 Gain, efficiency and bandwidth characteristics of the dipole antenna loaded with different DNG inclusions

Design type	Design I				Design II				Design III			
	f_{r1}	f_{r2}	f_{r3}	f_{r4}	f_{r1}	f_{r2}	f_{r3}	f_{r4}	f_{r1}	f_{r2}	f_{r3}	f_{r4}
centre requency, GHz	0.26	0.8	1.0	1.1	0.33	0.7	0.93	1.02	0.29	0.8	1.0	1.1
gain, dBi	−7.2	1.25	0.0	2.1	1.3	2.1	1.9	3.4	−3.5	2.0	0.5	2.2
efficiency, %	12.2	78	65	91	84	99	100	100	25	91	80	95
bandwidth, %	5.6	7.5	5.4	21.8	1.1	13.1	2.4	1.5	4.5	12.1	5	1.8

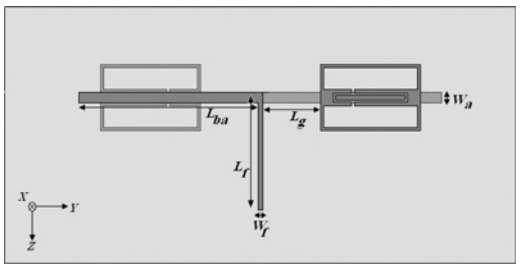

Fig. 6 *Printed dipole symmetrically loaded with single-cell MTM: $L_{ba} = 42.05$ mm, $L_f = 27.5$ mm, $L_g = 12.52$ mm, $W_a = 2.5$ mm and $W_f = 0.8$ mm*

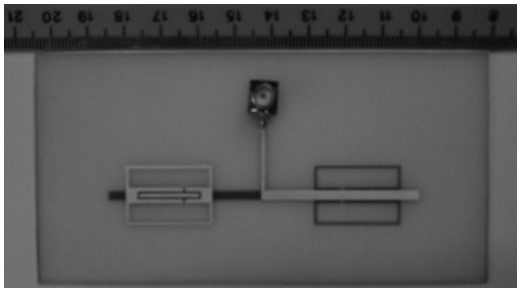

Fig. 7 *Prototype of proposed miniaturised printed dipole antenna loaded with single-cell MTM*

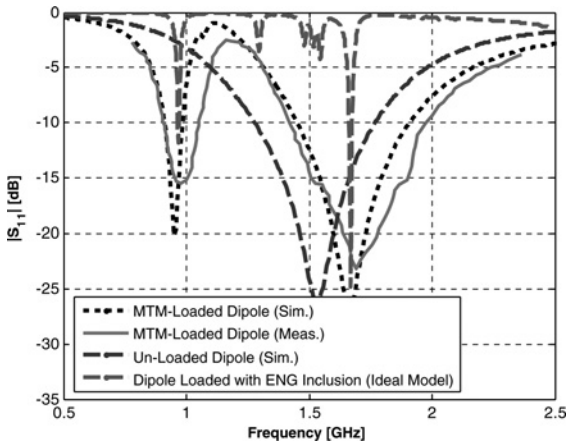

Fig. 8 *Return loss of the proposed miniaturised printed dipole antenna loaded with single-cell MTM*

As a reference, an unloaded dipole and an ideal model of the ENG-loaded dipole are also simulated

where

$$\mathrm{Im}(n) \geq 0, \quad e^{ink_0 d} = \frac{S_{21}}{1 - S_{11}(z - 1/z + 1)} \tag{3}$$

The ambiguity of the value of m in (2) is resolved by using Kramers–Kronig (KK) relating the real and imaginary parts

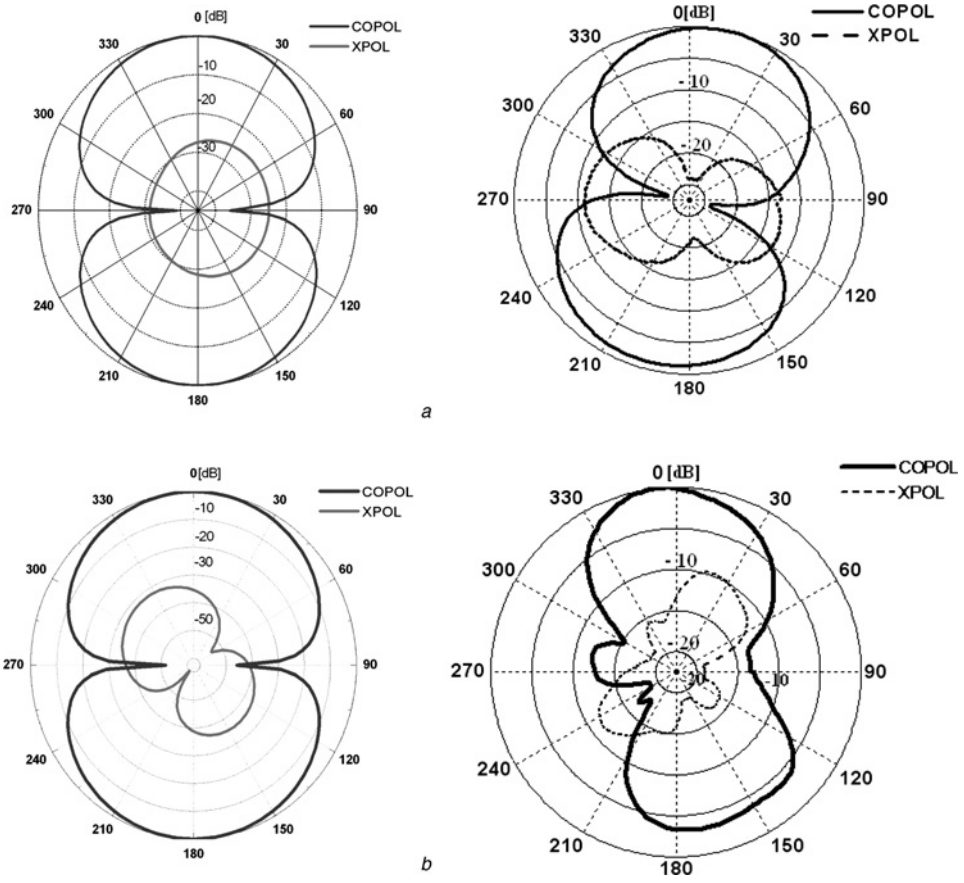

Fig. 9 *Radiation patterns of the proposed printed dipole antenna at*

a 940 MHz and

b 1.7 GHz (right-handed figures are measurements)

doi: 10.1049/iet-map.2010.0545

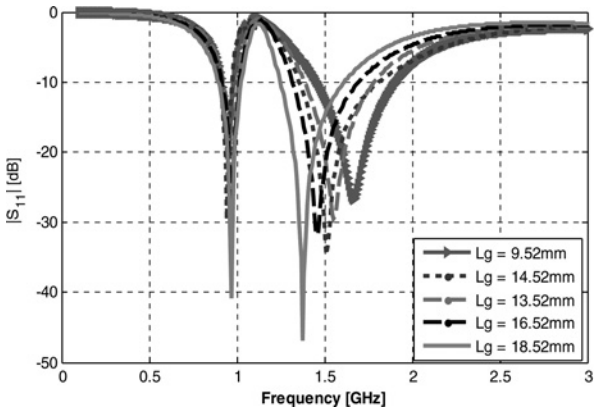

Fig. 10 *Effect of MTM location on the return loss of the printed dipole antenna*

of the index of refraction [16]

$$\mathrm{Re}(n(\omega)) = 1 + \frac{2}{\pi}\mathrm{P.V.}\left[\int_0^{\infty} \frac{\omega' \mathrm{Im}(n(\omega'))}{\omega'^2 - \omega^2}\, \mathrm{d}\omega'\right] \quad (4)$$

where, P.V. denotes the principal value of the integral. The effective permittivity (ε) and permeability (μ) of the medium can be expressed as: $\varepsilon = n/z$, $\mu = nz$. Fig. 5 shows the retrieved effective parameters of the proposed MTM cell. As can be seen, the proposed MTM cell has the permittivity that exhibits Drude behaviour at frequencies lower than 1.1 GHz and Lorentz behaviour [14] at frequencies higher than 1.1 GHz. Thus, this MTM can be approximated via a combination of Lorentz and Drude models.

4 Compact printed dipole antenna loaded with proposed MTM cells

In order to realise the miniaturisation method described in Section 2, double-sided printed dipole antenna is chosen for its simplicity in implementation and its low profile. Fig. 6 shows the proposed miniaturised printed dipole, in which a pair of proposed MTM cells is symmetrically added to each side of the printed dipole. The proposed MTM cells and dipole are printed on an FR4 substrate with a thickness of 0.8 mm and a dielectric constant of 4.4 to reduce the cost of the antenna and to make it more rigid in construction. For the MTM cells that are far away from the dipole arms, the coupling levels of them with the dipole arms are low and thus the arrangement of the several MTM cells has no effect on the frequency behaviour of the proposed antenna. As a result, the dipole is just loaded with single-cell MTM. Similar to the DNG-[3] and ENG-[17] MTMs, the proposed MTM cell can be modelled as a parallel resonant LC circuit. Thus, the proposed MTM cell is modelled as a resonant LC circuit parallel to the dipole, and the radiation into the free space is modelled as a resistor [18]. A prototype of the proposed miniaturised dual-band printed dipole is fabricated to confirm the simulation results. Fig. 7 shows a photograph of the fabricated antenna. Fig. 8 shows the return loss of the proposed symmetrically loaded dipole with the gap length, g_1, of 0.8 mm as well as the unloaded dipole antenna. As can be seen, the dipole antenna along with the loading elements provides good matching at both resonance frequencies. For comparison purposes, a simple dipole antenna loaded with lossy ENG inclusions, with the same retrieved effective parameters of the proposed MTM cell (see Fig. 5), is also simulated. As can be seen from Fig. 8, the return loss of the dipole loaded with ENG inclusions correlates nicely to that obtained for the single-cell MTM-loaded dipole. The co-polarised and cross-polarised radiation patterns of the proposed loaded dipole are measured at the resonant frequencies of 940 and 1.7 GHz. The measured and simulated radiation patterns at first and second resonant frequencies are shown in Fig. 9. As expected, the radiation patterns at both resonant frequencies are similar to that of the conventional unloaded dipole antenna.

The gain of the proposed antenna at low resonant frequency is high compared with that of the other miniaturised MTM-loaded dipoles [6–9]. The antenna gains at first and second resonant frequencies are −2.679 and 1 dBi, respectively. The proposed antenna has a broad bandwidth of 15.96% at 940 MHz (which is significantly wider than the bandwidth of other miniaturised MTM-loaded dipoles [6–9]) and 32.35% at 1.7 GHz. An important advantage of the proposed antenna is that the dipole length does not need to be increased to lower the resonant frequency. Consequently, a compact antenna is obtained.

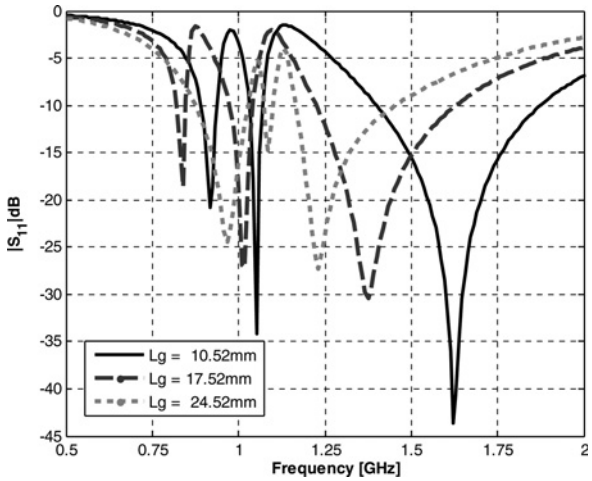

Fig. 11 *Simulated return loss of the proposed tri-band printed dipole symmetrically loaded with MTM cells*

Table 2 Comparison of the gain, bandwidth and efficiency for the loaded dipole antenna with different MTM locations

L_g	9.52 mm		13.52 mm		14.52 mm		16.52 mm		18.52 mm	
	f_{r1}	f_{r2}	f_{r1}	f_{r2}	f_{r1}	f_{r2}	f_{r1}	f_{r2}	f_{r1}	f_{r2}
centre frequency, GHz	0.95	1.68	0.96	1.59	0.95	1.51	0.96	1.5	0.94	1.39
gain, dBi	−2.38	1	−2.3	0.7	−2.5	0.55	−2.36	0.3	−2.7	0.14
effeciency, %	88	93	97	94	90	93	92	92	87	93
bandwidth, %	8.1	27	9.7	27	8.9	27	11.5	25	7.3	21

Table 3 Comparison of the gain, bandwidth and efficiency for the tri-band printed dipoles proposed in Section 5.1

L_g	10.52 mm			17.52 mm			24.52 mm		
	f_{r1}	f_{r2}	f_{r3}	f_{r1}	f_{r2}	f_{r3}	f_{r1}	f_{r2}	f_{r3}
centre frequency, GHz	0.92	1.05	1.64	0.84	1.01	1.43	0.96	1.09	1.3
gain, dBi	−3.4	−3.2	0.8	−3.7	−2.1	0.2	−1.7	−2.2	−0.4
effeciency, %	80	70	93	78	87	93	96	74	93
bandwidth, %	5.6	3.2	28	3	6.8	28.6	16.1	4.6	22.1

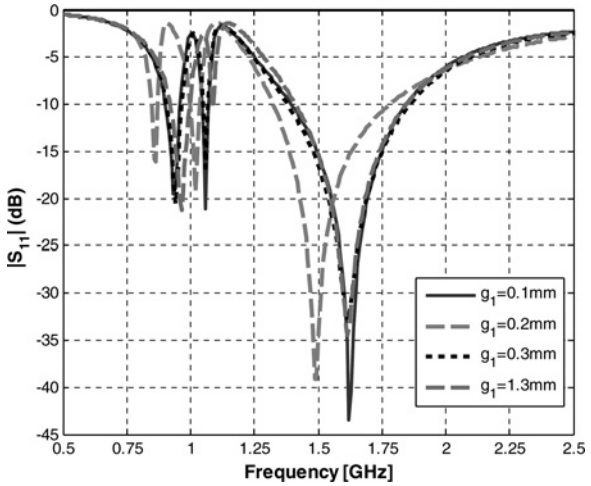

Fig. 12 *Simulated return loss of the proposed tri-band printed dipole (with $L_g = 12.52$ mm) asymmetrically loaded with MTM cells*

g_1 (see Fig. 4) for the right-hand MTM cell is fixed at 0.8 mm and g_1 for the left-hand MTM cell is changed

Finally, the effect of the MTM location is investigated to obtain some engineering guidelines for loaded dipole designs. Thus, the loading elements move along the antenna arms and the antenna return loss is plotted in Fig. 10 for each stage. The gain, bandwidth and efficiency of the loaded dipoles with different MTM locations are also compared in Table 2. As can be seen, the first resonant frequency remains approximately unchanged while the second one reduces as the MTM cells move away from the antenna feed point. Thus, when the MTM elements move closer to the dipole ends, the separation of the two resonances decreases. In addition, when the MTM cells are placed close to the antenna feed point, the proposed antenna cannot match very well to a 50 Ω transmission line. Moreover, as can be seen from Figs. 2 and 10, the single-cell MTM-loaded printed dipole follows closely the frequency behaviour of the dipole antenna loaded with cylindrical dispersive ENG-inclusions, as d_{MIF} or L_g increases.

5 Compact tri-band printed dipole antenna

In the previous design, a printed dipole was symmetrically loaded with single-cell MTMs to realise a dual-band operation. In this section, the design parameters of the proposed dual-band antenna are changed to provide a tri-band dipole antenna. As a result, two different tri-band printed dipoles are provided in the following subsections. Since changing the locations and dimensions of the MTM cells does not have any significant effect on the antenna radiation patterns, the proposed antennas radiate omnidirectional radiation patterns at all resonant frequencies. However, these are not plotted here for the sake of brevity.

5.1 Symmetrical loading

As revealed in Section 2, multi-resonance behaviour can be obtained by tuning the ENG-inclusion locations. As a result, the locations of the MTM cells on the dipole arms are changed in an attempt to realise tri-band printed dipole. Fig. 11 shows the return loss of the proposed tri-band printed dipole antenna with the cell's location as a parameter. As can be seen, for the certain locations of the MTM cells, a tri-band printed dipole can be achieved. The gain, efficiency and bandwidth of the proposed tri-band printed dipoles are compared in Table 3. As can be seen, the antenna gains at the low resonant frequencies are quite good.

5.2 Asymmetrical loading

In this subsection, effect of asymmetrical loading on the frequency behaviour of the printed loaded dipole is investigated to realise a tri-band dipole antenna. The simplest method to asymmetrically load a dipole antenna is to use two MTM cells with different gap widths (g_1 in Fig. 4). To this aim, a printed dipole antenna loaded with two MTM cells with different gap widths, g_1, is designed and simulated. The simulated return loss of the asymmetrical loaded dipole is shown in Fig. 12. In Fig. 12, the gap width of the first cell is fixed at 0.8 mm, and the return loss against frequency is plotted with the gap width of the second cell as

Table 4 Comparison of the gain, bandwidth and efficiency for the tri-band printed dipoles proposed in Section 5.2

g_1	0.1 mm			0.2 mm			0.3 mm			1.3 mm		
	f_{r1}	f_{r2}	f_{r3}	f_{r1}	f_{r2}	f_{r3}	f_{r1}	f_{r2}	f_{r3}	f_{r1}	f_{r2}	f_{r3}
centre frequency, GHz	0.93	1.06	1.62	0.86	1.02	1.56	0.94	1.06	1.62	0.96	1.09	1.63
gain, dBi	−3.5	−4.4	0.87	−3.9	−2.9	0.67	−3.5	−4.9	0.8	−2.9	−5.5	0.9
effeciency, %	81	57	93	79	78	94	82	52	92	86	43	93
bandwidth, %	6.4	3.2	28.3	2.9	4.2	30	6.3	2.4	30	8.5	1.4	26.7

doi: 10.1049/iet-map.2010.0545

a parameter. The gain, efficiency and bandwidth of the proposed tri-band printed dipoles are compared in Table 4. As can be seen, the antenna gains at the low resonant frequencies are reasonably good. As revealed in Fig. 12, the use of an asymmetric loading, formed by incorporating different resonant inclusions, leads to a third resonant frequency between the resonant frequencies of the symmetric loaded dipole. Thus, by adjusting the design parameters of the MTM cells, compact multi-band dipole antennas can be obtained. As a result, the gap capacitance of the MTM cell plays an important role in affecting the low resonance frequency. Thus, the proposed loading element can be integrated with varactor diode to provide an opportunity to design reconfigurable antennas with adjustable resonant frequencies.

6 Conclusion

The behaviour of a dipole antenna loaded with MTM inclusions has been examined. It has been revealed that embedding DNG-/ENG-inclusions in a simple dipole antenna can provide an opportunity to design multi-band antenna. In order to realise this method, a single unit cell of MTM reactive loading has been utilised. Results show that placing proposed MTM cells in close proximity of a printed dipole antenna creates a double resonant antenna, the response of which is a function of MTM dimensions as well as of locations of MTM cells along the dipole arms. Compact tri-band printed dipole antennas have also been designed by symmetrically and asymmetrically loading of the printed dipole. A prototype of the proposed dual-band MTM-loaded printed dipole is fabricated to validate the simulation result. A good agreement between the measured and simulated results is achieved.

7 References

1 Rogers, S.D., Butler, C.M., Martin, A.Q.: 'Design and realization of GA-optimized wire monopole and matching network with 20:1 bandwidth', *IEEE Trans. Antennas Propag.*, 2003, **51**, (3), pp. 493–502

2 Erentok, A., Luljak, P., Ziolkowski, R.W.: 'Antenna performance near a volumetric metamaterial realization of an artificial magnetic conductor', *IEEE Trans. Antennas Propag.*, 2005, **53**, pp. 160–172

3 Ziolkowski, R.W., Kipple, A.: 'Application of double negative metamaterials to increase the power radiated by electrically small antennas', *IEEE Trans. Antennas Propag.*, 2003, **51**, (10), pp. 2626–2640

4 Liu, Q., Hall, P.S., Borja, A.L.: 'Efficiency of electrically small dipole antennas loaded with left-handed transmission lines', *IEEE Trans. Antennas Propag.*, 2009, **57**, (10), pp. 3009–3017

5 Jafargholi, A., Kamyab, M., Veysi, M.: 'Artificial magnetic conductor loaded monopole antenna', *IEEE Antennas Wirel. Propag. Lett.*, 2010, **9**, pp. 211–214

6 Iizuka, H., Hall, P.S., Borja, A.L.: 'Dipole antenna with left-handed loading', *IEEE Antennas Wirel. Propag. Lett.*, 2006, **5**, pp. 483–485

7 Borja, A.L., Hall, P.S., Liu, Q., Iizuka, H.: 'Omnidirectional left-handed loop antenna', *IEEE Antennas Wirel. Propag. Lett.*, 2007, **6**, pp. 495–498

8 Iizuka, H., Hall, P.S.: 'Left-handed dipole antennas and their implementations', *IEEE Trans. Antennas Propag.*, 2007, **55**, (5), pp. 1246–1253

9 Rafaei Booket, M., Kamyab, M., Jafargholi, A., Mousavi, S.M.: 'Analytical modeling of the printed dipole antenna loaded with CRLH structures', *Prog. Electromagn. Res. B*, 2010, **20**, pp. 167–186

10 Zhu, J., Antoniades, M.A., Eleftheriades, G.V.: 'A compact tri-band monopole antenna with single-cell metamaterial loading', *IEEE Trans. Antennas Propag.*, 2010, **58**, (4), pp. 1031–1038

11 Mosallaei, H., Sarabandi, K.: 'Design and modeling of patch antenna printed on magneto-dielectric embedded-circuit metasubstrate', *IEEE Trans. Antennas Propag.*, 2007, **55**, (1), pp. 1031–1038

12 Tretyakov, S.A., Maslovski, S.I., Sochava, A.A., Simovski, C.R.: 'The influence of complex material coverings on the bandwidth of antennas', Proc. URSI 2004 Int. Symp. Electromagnetic Theory, Pisa, Italy, 23–27 May, 2004, vol. 1, pp. 99–101

13 Balanis, C.A.: 'Advanced engineering electromagnetics' (Wiley, New York, 1989)

14 Engheta, N., Ziolkowski, R.: 'Metamaterials: physics and engineering explorations' (John Wiley & Sons Inc., 2006)

15 Veysi, M., Kamyab, M., Mousavi, S.M., Jafargholi, A.: 'Wideband miniaturized polarization-dependent HIS incorporating metamaterials', *IEEE Antennas Wirel. Propag. Lett.*, 2010, **9**, pp. 764–766

16 Lucarini, V., Saarinen, J.J., Peiponen, K.-E., Vartiainen, E.M.: 'Kramers–Kronig relation in optical materials research' (Springer Series in Optical Sciences, 2005, vol. 110)

17 Alu, A., Engheta, N.: 'Pairing an epsilon-negative slab with a mu-negative slab: resonance, tunneling and transparency', *IEEE Trans. Antennas Propag.*, 2003, **51**, pp. 2558–2571

18 Sievenpiper, D.: 'Chapter11: review of theory, fabrication, and applications of high impedance ground planes', in Engheta, N., Ziolkowski, R. (Eds.): 'Metamaterials: physics and engineering explorations' (John Wiley & Sons Inc., 2006)